Journal of
Composites Science

MDPI

Article

Non-Isothermal Crystallization Kinetic of Polyethylene/Carbon Nanotubes Nanocomposites Using an Isoconversional Method

Beatriz Rossi Canuto de Menezes *, Tiago Moreira Bastos Campos, Thais Larissa do Amaral Montanheiro, Renata Guimarães Ribas, Luciana de Simone Cividanes and Gilmar Patrocínio Thim

Technological Institute of Aeronautics, Division of Fundamental Sciences, Laboratory of Plasmas and Process, São José dos Campos, SP 12.228-900, Brazil; moreiratiago22@gmail.com (T.M.B.C.); tlamontanheiro@gmail.com (T.L.d.A.M.); rguimaraes42@gmail.com (R.G.R.); lu_civi@yahoo.com.br (L.d.S.C.); gpthim@gmail.com (G.P.T.)

* Correspondence: beatriz1menezes@gmail.com; Tel.: +55-12-3947-5958

Received: 30 January 2019; Accepted: 14 February 2019; Published: 18 February 2019

Abstract: Behavior studies of thermoplastic polymers during non-isothermal crystallization are extremely important since most of their properties are influenced by degree of crystallinity and the crystallization process. In general, an approach based on a model-fitting method is used to perform crystallization kinetic studies. Due to their inability to uniquely determine the reaction mode, many studies have used the isoconversional method, where it is not necessary to assume a crystallization model to obtain the kinetic parameters. Therefore, in this work, the influence of acid and octadecylamine functionalized carbon nanotubes (CNTs) in the crystallization kinetic of polyethylene (PE) was studied using an isoconversional method with differential scanning calorimetry (DSC) and polarized optical microscopy (POM). The kinetic parameters and the crystallization model were determined. The incorporation of functionalized and non-functionalized CNTs into PE did not change the Johnson-Mehl-Avrami crystallization model. However, the CNTs increased the crystallization temperature and reduced the activation energy for crystallization. In addition, the Avrami coefficient values were lower for the nanocomposites when compared to pure PE. The incorporation of CNTs accelerated the crystallization of PE, reducing the crystallite sizes and modifying their morphology.

Keywords: carbon nanotubes; high-density polyethylene; crystallization kinetic; isoconversional method; functionalization

1. Introduction

The use of plastics in several areas became widespread after World War II, rapidly increasing the production and even surpassing the commercialization of most other materials, especially metals. From then on, a world without the use of synthetic organic polymers seems inconceivable. Polyethylene (PE) is the most consumed polymer, accounting for about 36% of production [1,2]. PE presents interesting properties, such as chemical inertness, low permeability, corrosion resistance, good stiffness, low density, and excellent electrical resistance. These qualities along with its low cost and easy processability make PE the choice material for a vast number of applications, especially for food packaging, storage containers for liquids, and chemical storage tanks [3].

Despite the outstanding properties of PE, some disadvantages, such as low operating temperature and some poor mechanical properties, limit its potential use inhigh-technological engineering applications [4,5]. The incorporation of nanofillers is an option to overcome these drawbacks. Carbon

nanotubes (CNTs) have been widely studied as nanocomposite fillers since their popularization with the publication of Iijima in 1991 [6,7]. CNTs remarkable properties, such as high Young's modulus and tensile strength, chemical stability, biocompatibility, and excellent thermal conductivity, make them attractive for reinforcing polymer matrix, increasing the mechanical, biological, and thermal properties of the nanocomposite [8–10].

Understanding the interaction between the polymeric matrix and the filler is crucial to obtain a material with the desired properties. An effective dispersion of CNTs and a proper polymer–filler interaction are necessary to achieve the best performance of nanocomposites. Several techniques have been used to improve the dispersion and interaction of CNTs in polymeric matrix, including optimum physical blending, in situ polymerization, and chemical functionalization [11]. Physical blending breaks the CNT bundles through shear stress. Mechanical stirring, sonication, shear mixing, and ball milling are some processes used to optimize the CNT/polymer physical blending [12]. Another interesting approach to enhance the dispersion and interaction of CNTs with polymers is in situ polymerization. In this process, conjugated polymers are attached to CNT surfaces, acting as an initial local to the olefin monomers polymerization [11,13].

Chemical functionalization has been used in many studies to improve dispersion and guarantee the CNTs interaction with the polymeric matrix. The most common surface modification uses a mixture of concentrated nitric (HNO_3) and sulfuric acids (H_2SO_4) to produce reactive carboxylic groups (-COOH) on the CNTs sidewalls and ends. -COOH groups can react with a large number of other chemical compounds, attaching a functional group suitable to better dispersion and interaction properties, depending on the polymeric matrix [14]. Different reactive chemical groups can be used, such as alkyl, phenyl, amide, ester, silanes, thiol, and biomolecules [15]. Non-covalent functionalization, through weak van der Waals interactions, can also be used to modify the CNTs, without any damage to their structure and properties. In this case, ionic liquids, biomolecules, and other chemical compounds are adsorbed on CNT surfaces, shielding the stacking interactions [15,16]. Since polyethylene has a nonpolar character, the use of covalent functionalization with long-chain amines for CNTs provides a better interaction with this polymer [17].

The incorporation of a filler into a polymeric matrix will considerably affect the crystallization behavior. Alterations to the polymer chain configuration, glass transition temperature (T_g) and melt temperature (T_m), the rate of crystal formation, crystallite shape and size, activation energy (E_a), and crystallization mechanism are some effects that CNTs can cause when they are added into PE [18,19]. In this way, the influence of CNTs in the crystallization kinetic of PE is a subject of interest for many research groups, since it will affect the industrial process and the final properties of the polymer [20]. Thermogravimetric analysis (TGA) and differential scanning calorimetry (DSC) are the main techniques used to perform kinetic studies.

Many studies have investigated the crystallization kinetic of composites based on PE. Tarani et al. [21] investigated the effect of incorporating graphene nanoplatelets with an average thickness of 10 nm and different sizes (5, 15, and 25 μm) in diameter on the crystallization kinetics of high-density polyethylene (HDPE) under non-isothermal conditions. Different models were tested, and the authors showed that the Avrami analysis modified by Jeizorny and the Mo method described very well the non-isothermal crystallization of the nanocomposites. The addition of graphene changed the overall crystallization rate and the E_a.

Shehzad et al. [22] synthesized HDPE/graphene nanocomposites and studied the non-isothermal crystallization using the Jeizorny-modified Avrami model, Ozawa model, and the model proposed by Mo. The results showed that graphene nucleated the crystallization of HDPE, decreasing E_a and increasing the crystallization onset temperature (Ton). The Jeizorny and Ozawa models failed to describe the crystallization kinetics. On the other hand, the model developed by Mo successfully described the non-isothermal process of the HDPE and the nanocomposites.

Sahoo et al. [23] studied the crystallization kinetic of low-density polyethylene (LDPE) and silver nanoparticles (Ag-NPs) using DSC. Different kinetic models, such as Avrami, Malkin, and Mo,

were used to analyze the non-isothermal crystallization behavior of the LDPE and the nanocomposites. The results showed that the polymer and nanocomposites followed the Avrami and Malkin models. The authors concluded that Ag-NPs influenced the LDPE crystallization kinetic. For pure LDPE, only a primary crystallization was observed, while the nanocomposite presented both primary and secondary crystallization. In addition, the Avrami exponent also changed. Fan et al. [24] prepared nanocomposites of PE/montmorillonite and analyzed the kinetic behavior of PE and the nanocomposites by Avrami and Hoffman models. The results showed that montmorillonite acted as a nucleating agent in the solidification process, reducing the average size of spherulites. However, the nanoparticles did not change the crystallinity of PE.

Previous research used model-fitting methods to perform non-isothermal crystallization kinetic analysis. Although widely used, model-fitting methods present several problems, especially concerning their inability to uniquely determine the reaction model [25]. Additionally, they assume a constant kinetic triplet (A, E_a, and model), which are simultaneously fitted from a single curve. Furthermore, the model-fitting method involves a single heating rate, which is not sufficient to study kinetic reactions. Isoconversional models overcome these limitations since the kinetic is evaluated without modelistic assumptions [26]. In this method, kinetic parameters, such as E_a, can be estimated using the degree of conversion (α) as a function of the heating rate [27].

A significant gap in polymeric kinetic studies still remains. Most studies use a model-fitting method for the kinetic calculation of polymer crystallization. There are very few studies in which the isoconversional method is used for crystallization analysis of polymers and polymeric composites, especially for polyethylene and carbon nanotubes. Thus, there is considerable potential for the application of the isoconversional method crystallization kinetics in the study of HDPE/CNT nanocomposites, which may contribute to a better understanding of the influence of CNTs on the final properties of the nanocomposite.

Similar work has already been performed by our group in the study of mullite crystallization. The isoconversional and non-isothermal Flynn-Wall-Ozawa method was used to analyze the effect of different amounts of urea in the production and crystallization of mullite. Using this method, the kinetic model, kinetic parameters, and activation energy were measured, resulting in a great understanding of the relation between mullite crystallization, structure, and properties [28]. Although commonly used in ceramic material crystallization studies, this method has not been very well applied in polymers. The objective of the present work is thus to compare the non-isothermal crystallization kinetics of pure HDPE and its nanocomposites with acid and octadecylamine-functionalized CNTs. The non-isothermal crystallization data was obtained by differential scanning calorimetry (DSC), and the isoconversional method was used to study the crystallization kinetics, defining the reaction model and calculating the kinetic parameters. Polarized optical microscopy (POM) was performed to verify the results obtained by kinetic analysis. To the best of our knowledge, there are no other works using the isoconversional method to study the kinetic crystallization of HDPE or HDPE/CNT nanocomposites.

2. Theoretical Background

The rate of polymer crystallization can be described using the general equation of solid-state reactions,

$$\frac{d\alpha}{dt} = kf(\alpha) \tag{1}$$

where α is the conversion fraction, t is the time, k is the reaction rate constant, and $f(\alpha)$ is the reaction model. The mechanism controlling the reaction, along with the size and shape of the reactive particles will define $f(\alpha)$ [29]. Table 1 lists several reaction models with their mechanisms and equations for $f(\alpha)$.

Kinetic calculations from DSC curves use the following equation to calculate α:

$$\alpha = \frac{A_i}{A_t} \tag{2}$$

where A_i is the area under the crystallization peak to a T_i temperature and A_t is the total area. Integrating Equation (1) gives the integral rate law representative of the reaction model, $g(\alpha)$,

$$g(\alpha) = kt \tag{3}$$

Table 1. Solid-state rate expressions for distinct reaction models.

Model	Mechanism	$f(\alpha)$
Šesták and Berggren (SB) [30]	Autocatalytic, General mechanism	$\alpha^m(1-\alpha)^n$
Johnson-Mehl-Avrami (JMA) [31]	Nucleation and growth	$n(1-\alpha)[-\ln(1-\alpha)]^{1-\frac{1}{n}}$
Reaction Order (RO) [32,33]	One-parameter model	$(1-\alpha)^n$
Polany-Winger (R1) [34–36]	Phase boundary-controlled reaction (one-dimensional)	*Constant*
Contracting cylinder (R2) [32,35]	Phase boundary-controlled reaction (contracting area)	$2(1-\alpha)^{1/2}$
Contracting sphere (R3) [34,35]	Phase boundary-controlled reaction (contracting volume)	$3(1-\alpha)^{2/3}$
Parabolic Law (D1) [36]	Diffusion (one-dimensional)	$1/(2\alpha)$
Valenci (D2) [36]	Diffusion (two-dimensional)	$[-\ln(1-\alpha)]^{-1}$
Jander (D3) [36]	Diffusion (three-dimensional)	$3(1-\alpha)^{\frac{1}{3}}/2[(1-\alpha)^{-\frac{1}{3}}-1]$
Brounshtein-Ginstling (D4) [36]	Diffusion (four-dimensional)	$3/2[(1-\alpha)^{-\frac{1}{3}}-1]$

The dependence of temperature on the rate of crystallization reaction is defined by the Arrhenius equation,

$$k = Ae^{\frac{-E_a}{RT}} \tag{4}$$

where A is the pre-exponential ("frequency") factor, E_a is the activation energy, T is the absolute temperature, and R is the gas constant [37]. Substituting Equation (4) in the rate expression from Equation (1) and the integrated rate expression from Equation (3) gives,

$$\frac{d\alpha}{dt} = Ae^{\frac{-E_a}{RT}} f(\alpha) \tag{5}$$

and

$$g(\alpha) = Ae^{\frac{-E_a}{RT}} t \tag{6}$$

In order to obtain the kinetic parameters from non-isothermal crystallization reactions, the rate expressions must be transformed by,

$$\frac{d\alpha}{dT} = \frac{d\alpha}{dt}\frac{dt}{dT} \tag{7}$$

being that

$$\frac{dt}{dT} = \frac{1}{\beta} \tag{8}$$

where $d\alpha/dT$ is the non-isothermal crystallization rate, $d\alpha/dt$ is the isothermal crystallization rate, and β is the heating rate. Substituting Equations (5) and (8) into Equation (7) gives the differential expression of the non-isothermal rate law,

$$\frac{d\alpha}{dT} = \frac{A}{\beta}e^{\frac{-E_a}{RT}} f(\alpha) \tag{9}$$

Integrating Equation (9) gives,

$$g(\alpha) = \frac{A}{\beta}\int_0^T e^{\frac{-E_a}{RT}}dT \tag{10}$$

Substituting E_a/RT by "x" and changing the integral limits, Equation (10) becomes,

$$g(\alpha) = \frac{AE_a}{\beta R}\int_x^\infty \frac{e^{-x}}{x^2}dx \tag{11}$$

Equation (11) can be written as,

$$g(\alpha) = \frac{AE_a}{\beta R}p(x) \tag{12}$$

where $p(x)$ is the exponential integral [27],

$$p(x) = \int_x^\infty \frac{e^{-x}}{x^2}dx \tag{13}$$

The exponential integral $p(x)$ has no analytic solution, but many approximations. The Flynn-Wall-Ozawa method is an isoconversional method that uses Doyle's linear approximation for $p(x)$ [38], whereby Equation (12) is transformed into,

$$\log\beta = \log\frac{AE_a}{g(\alpha)R} - 2.315 - 0.457\frac{E_a}{RT} \tag{14}$$

Differentiating and assuming α constant,

$$\frac{d\log\beta}{d(1/T)} = -\left(\frac{0.457}{R}\right)E_a \tag{15}$$

Thus, the plot of $\log\beta$ versus $1/T$, for each α, gives E_a from the angular coefficient of the curve. In this way, the activation energy is calculated for each conversion fraction [27]. In addition, the crystallization mechanism for each heating rate can be determined using the kinetic compensation effect [39]. The pre-exponential factor (A) can be determined by Kissinger Method for a first-order reaction, that is $f(\alpha) = 1-\alpha$. Substituting $f(\alpha)$ in Equation (9),

$$\frac{d\alpha}{dT} = \frac{Ae^{\frac{-E_a}{RT}}}{\beta}(1-\alpha) \tag{16}$$

Deriving Equation (16) and equaling to zero (when the reaction rate is maximum),

$$\frac{E_a}{RT_m^2} = \frac{d\alpha}{dT} + \frac{\alpha E_a}{RT_m^2} \tag{17}$$

where T_m is the maximum temperature of the DSC peak. Substituting Equation 16 into Equation (17),

$$A = \frac{\beta E_a e^{E_a/RT_m}}{RT_m^2} \tag{18}$$

Equation (18) allows the calculation of A for each conversion fraction. If E_a does not vary with α, the reaction occurs in a single step. On the other hand, a complex mechanism is assumed if E_a varies with α [36].

The values of ln$A$ and Ea have a linear relationship, known as the kinetic compensation effect. Such linearity indicates that the proposed kinetic model is the same in the studied range. The effect of kinetic compensation is expressed by Equation (19) [40,41],

$$\ln A = a + (bE_a) \tag{19}$$

where a and b are constants.

To obtain the kinetic model of the studied reaction, it is necessary to obtain the functions $y(\alpha)$ and $z(\alpha)$, which are defined by Ozawa [42,43] as,

$$\frac{d\theta_t}{dt} = e^{\frac{-E_a}{RT}} \tag{20}$$

where θ_t is generalized time, denoting the reaction time taken to reach a distinct α at infinite temperature [44].

Combining Equations (5), (8), and (20), the following expression is obtained [44,45],

$$y(\alpha) = \frac{d\alpha}{d\theta_t} = Af(\alpha) = \frac{d\alpha}{dT}\beta e^{\frac{E_a}{RT}} \tag{21}$$

where $d\alpha/d\theta_t$ corresponds to the generalized rate of reaction and is obtained by extrapolation of $d\alpha/dt$ to an infinite temperature. Integrating Equation (21),

$$g(\alpha) = \int_0^{\alpha} \frac{d\alpha}{f(\alpha)} = A\int_0^{\theta_t} d\theta_t = A\theta_t \tag{22}$$

Combining Equations (21) and (22), a general expression for $z(\alpha)$ is obtained [33],

$$z(\alpha) = y(\alpha)\theta_t = \frac{d\alpha}{d\theta}\theta_t = f(\alpha)g(\alpha) \tag{23}$$

Substituting Equation (20) into (23),

$$z(\alpha) = y(\alpha)\int \frac{e^{\frac{-E_a}{RT}}}{\beta} dT \tag{24}$$

Thus, the functions $y(\alpha)$ and $z(\alpha)$ can be determined, defining the reaction model by the derivative of these functions (a_y and a_z). Figure 1 shows different reaction models according to the values of a_y and a_z [32,33].

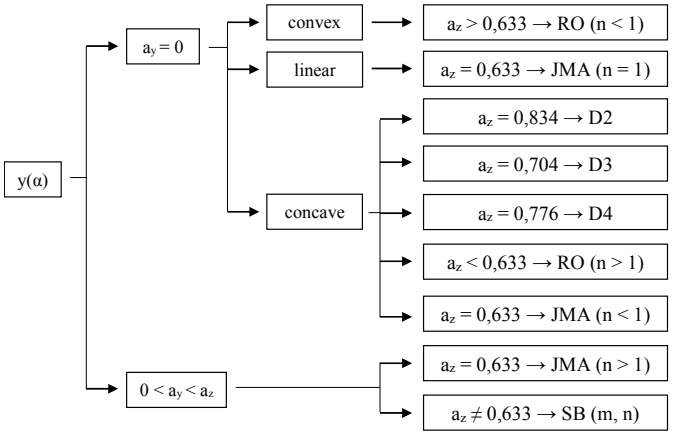

Figure 1. Schematic diagram of kinetic models using $y(\alpha)$ and $z(\alpha)$ functions (Adapted from [33,34]).

3. Materials and Methods

3.1. Materials

The HDPE pellets used in this study were obtained from Brasken (IG58, ρ = 0.956 gcm^3). The multi-walled CNTs used as a nanofiller to prepare HDPE nanocomposites were provided by INPE-Brazil and prepared by the chemical vapor deposition method (CNT–P) [46]. The acid (CNT–COOH) and octadecylamine (CNT–ODA) functionalization were performed following previous procedures [17].

3.2. Nanocomposite Preparation

The HDPE/CNT nanocomposites were prepared using pristine and functionalized CNTs (0.8% wt). First, CNTs were dispersed in a proper solvent (acetone for CNT–P and CNT–COOH, and cyclohexane for CNT–ODA) in an ultrasonic bath for 30 min. Then, HDPE pellets were mixed into solutions and kept under magnetic stirring for another 30 min. The solvent was removed in an oven at 80 °C for 24 h, leaving the remaining HDPE pellets covered with the nanotubes. The mixture of pellets/CNTs was melted in a heating mantle (Arsec AQ22B) at 210 °C, and after complete melting, was mechanically stirred (IKA RW 20) at 600 rpm for 1 min. The highly viscous solution was placed into aluminum molds and poured into a vacuum oven at 210 °C for 2 h with an absolute pressure of 0.2 bar to eliminate entrapped air. Subsequently, the samples were cast under compression (5 kgf) and cooled at ambient temperature. The samples prepared were labeled as HDPE Pure, HDPE/CNT–P, HDPE/CNT–COOH, and HDPE/CNT–ODA.

3.3. Differential Scanning Calorimeter (DSC)

The non-isothermal crystallization behavior of the HDPE and HDPE/CNT nanocomposites was measured by DSC with a Perkin Elmer, Pyris 1 calorimeter. Samples with low mass (10 mg) were poured inside aluminum pans and protected during DSC experiments by an inert atmosphere of N_2 to avoid thermal degradation. For the non-isothermal crystallization experiment, each sample was first melted to 220 °C at a heating rate of 10 °C/min for 5 min. This temperature is above the HDPE melting temperature (Tm = 125–132 °C [3]) to erase all previous thermal history. Specimens were then cooled to ambient temperature at four different heating rates: 5, 7, 10, and 15 °C/min. The exothermal curves obtained during the non-isothermal crystallization for various cooling rates were used to develop the kinetics study.

3.4. Polarized Optical Microscopy (POM)

POM was performed using a Leica DMLS microscope equipped with a Linkam THMSG 600 hot stage. The HDPE and HDPE/CNT nanocomposites were observed in the form of thin films that were prepared between a microscope coverslip by melting the polymer at 200 °C for 10 min and then cooling until the isotherm reached 127 °C. The images were recorded in the isotherm from time to time in order to analyze the crystallite growth until complete crystallization. Crystallite size measurements were performed using the image analysis program ImageJ, taking an average of 10 measures.

4. Results

4.1. Isoconversional Analysis of DSC Crystallization Data

The DSC cooling curves for HDPE and HDPE/CNT nanocomposites are shown in Figure 2. As expected, all curves present only one well-defined exothermal peak around 115–120 °C, corresponding to the HDPE crystallization. By increasing the cooling rate, the peak temperatures shift towards lower temperatures and become broader for all samples. At a lower cooling rate, the polymer chains have more fluidity and diffusivity. In this case, at a higher temperature, there is enough time for the chains to move from the melt to the crystallized surfaces. In contrast, when the cooling rate

increases, the motion of polyethylene chains is not able to follow the cooling temperature and there is no sufficient time to activate nuclei. Then, more supercooling is required to organize the chain into more perfect crystallites, resulting in a broadening of the curve [21,22].

The crystallization peak temperature (T_p), the onset temperature (T_{on}), and the absolute crystallinity (X_c) for each cooling rate (β) were determined and are showed in Table 2. The incorporation of carbon nanotubes to HDPE slightly increased T_{on} and T_p, which means that there are interactions between the filler and the matrix. The increase in T_{on} and T_p is related to an enhanced number of heterogeneous nuclei for crystallization. So, the functionalized and non-functionalized CNTs act as nucleating agents for HDPE crystals [47]. This result agrees with data derived from similar systems [48,49]. There was no significant difference in T_{on} and T_p between the used CNTs.

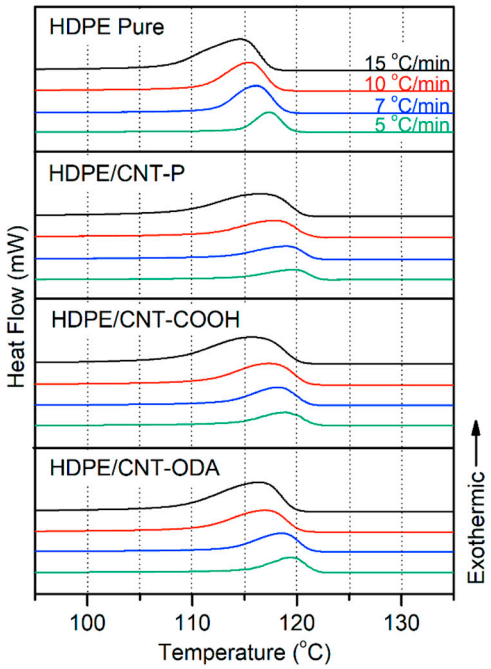

Figure 2. Differential scanning calorimetry (DSC) cooling curves at various cooling rates (5, 7, 10, and 15 °C/min) for pure high-density polyethylene (HDPE) and high-density polyethylene carbon nanotubes (HDPE/CNT) nanocomposites.

In addition, the HDPE and HDPE/CNT nanocomposites degree of crystallinity was about 64% and did not vary significantly with the CNTs. The incorporation of nanofillers into a polymer can increase, decrease, or maintain the absolute crystallinity, which will depend on whether the CNT will interfere more in the nucleation or in the growth process of polymeric crystals. If the incorporation of CNTs strongly induces the formation of more nucleation sites, an increase in the absolute crystallinity of HDPE is expected. On the other hand, CNTs can act as obstacles, hindering the mobility of HDPE chains. In this way, the folding of polymeric chains is difficult and, consequently, a decrease in absolute crystallinity is more likely. The interface between CNT/HDPE also interferes with the crystallinity, since it can produce an amorphous phase that will also interfere with the crystal growth. Another important factor is the CNT lengths, where longer CNTs reduce the mobility of polymeric chains. Our results showed that the chain mobilities of samples produced was hindered by CNT presence, which also induced the formation of new nucleation sites. In addition, the CNTs had no significant effect on absolute crystallinity of nanocomposites, which was the same when compared with pure HDPE [50,51].

Table 2. Summarized DSC results at various cooling rates (5, 7, 10, and 15 °C/min) for pure HDPE and HDPE/CNT nanocomposites.

Sample	β (°C/min)	T_{on} (°C)	T_p (°C)	X_c (%)
HDPE Pure	5	119	117	65
	7	119	117	64
	10	118	116	66
	15	117	115	65
HDPE/	5	122	120	62
CNT–P	7	122	119	61
	10	121	118	66
	15	121	116	65
HDPE/	5	122	119	65
CNT–COOH	7	121	118	63
	10	121	117	66
	15	120	116	64
HDPE/	5	122	119	64
CNT–ODA	7	121	119	64
	10	120	117	64
	15	120	116	63

The values of relative crystallinity at various cooling rates was calculated by integrating the exothermic peaks, using the following Equation [52]:

$$X_t = \frac{\Delta H(T)}{\Delta H_{total}} = \frac{\int_{T_0}^{T} \left(\frac{dH}{dT}\right) dT}{\int_{T}^{T_\infty} \left(\frac{dH}{dT}\right) dT} \quad (25)$$

where T_0, T, and T_∞ are the onset, arbitrary, and end crystallization temperatures, respectively, and dH is the heat released in an infinitesimal temperature interval dT. Relative crystallinity (X_t) as a function of temperature for HDPE and HDPE/CNT nanocomposites is shown in Figure 3. The sigmoidal curves shifted to the left side suggest that the polymer started to crystallize at lower temperatures and the crystallization increases as temperature decreases. This is because of the strong relationship between the nucleation/growth process and temperature. Before the inflection point (before the maximum DSC peak), a fast and primary process occurs, related to the nucleation and growth of the first PE crystals. After the maximum value of heat flow for the DSC peak, the crystallinity is developed by a slower and secondary kinetic process. The curves from Figure 3 also showed the influence of the cooling rate on crystallinity. At lower cooling rates, the samples presented more crystallinity at a higher temperature. In this case, the polymer chains have more fluidity and diffusivity due to the low viscosity and more time for secondary crystallization [53].

The isoconversional method of Friedman (logarithm of Equation (9) [54]) was used to evaluate the effective action of CNTs as a nucleation agent, and to identify the model and crystallization mechanism. The dependence of effective crystallization energy (E_a) on the relative crystallinity (α) was calculated and is presented in Figure 4. E_a is defined as the energy necessary for the motion of the polymeric crystalline chains across the phase [22]. For HDPE and HDPE/CNT nanocomposites, E_a is negative, suggesting that the crystallization increases as the temperature decreases. For both pure HDPE and nanocomposites, E_a increased with the relative crystallinity. This implies that as the relative crystallinity increases, it becomes more difficult for the polymeric system to continue crystallization [55].

The incorporation of CNT–P and CNT–COOH into HDPE significantly decreased the activation energy when compared to pure HDPE, showing that these CNTs can act effectively as a nucleating agent, accelerating the crystallization process [55]. The incorporation of CNT–ODA also reduced the activation energy, but not as effectively as CNT–P and CNT–COOH. By comparing the different nanocomposites, the reduction in activation energy follows the sequence HDPE/CNT–P <

HDPE/CNT–COOH < HDPE/CNT–ODA. This result can be related to two main factors: (i) dispersion of CNTs in polymeric matrix and (ii) interaction between HDPE and CNTs.

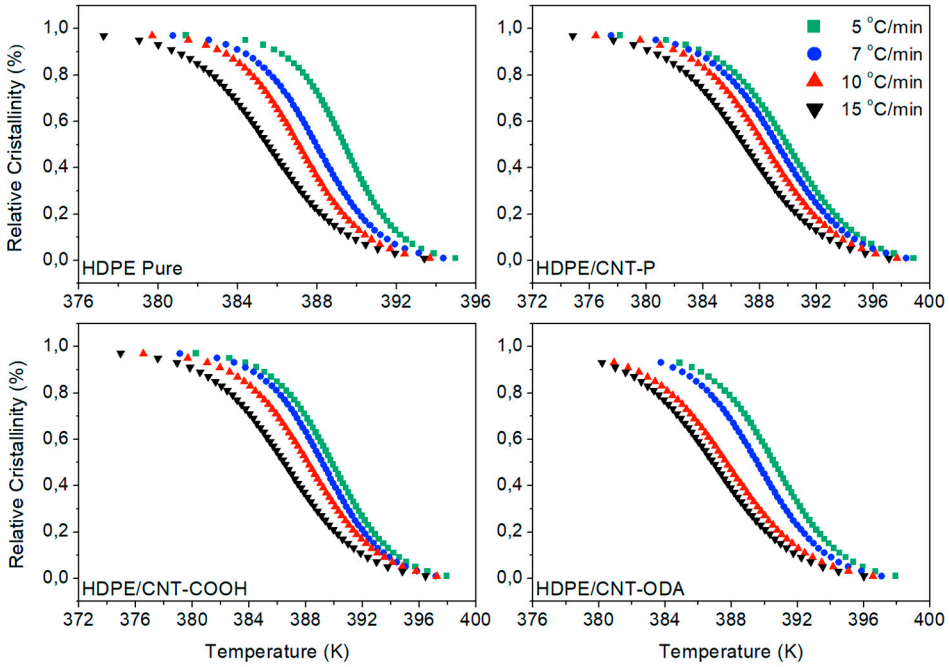

Figure 3. Temperature versus relative crystallinity at various cooling rates (5, 7, 10, and 15 °C/min) for pure HDPE and HDPE/CNT nanocomposites.

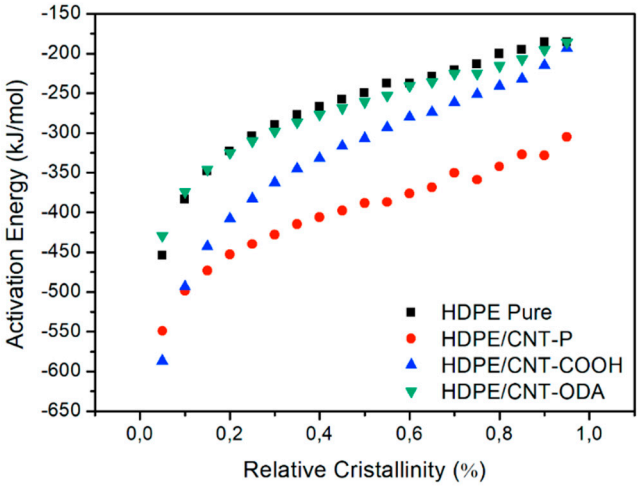

Figure 4. Activation energy versus relative crystallinity at various cooling rates (5, 7, 10, and 15 °C/min) for pure HDPE and HDPE/CNT nanocomposites.

Pristine CNTs tend to agglomerate and entangle together due to their large surface area and high van der Waals forces. After acid-functionalization, negative charges are created on CNT surfaces, that improve the dispersion but also increase the polar character. HDPE is a non-polar polymer, so the interaction with CNT–COOH is not as effective. Thus, for CNT–P and CNT–COOH, it is expected that the formation of large agglomerates will not interact properly with HDPE and will act more intensively as nucleating agents. The octadecylamine functionalization provided a better interaction and dispersion of CNT–ODA with the polymeric matrix due to two aspects: (i) the similarity of the HDPE chains with the structure of the octadecylamine (basically CH_2) and (ii) the non-polar character presented by both CNT–ODA and HDPE. Therefore, for HDPE/CNT–ODA, it is

expected that CNT–ODA will merge with the HDPE matrix due to the ODA chains, reducing the activity as nucleating agents. Our previous work [17] proved this effect. The better dispersion and interaction of CNT–ODA with HDPE produced more homogeneous nanocomposites with higher mechanical properties.

Using Equation (19), the existence of the compensation effect between values of E_a and ln$A$ was verified (Figure 5). All samples showed a correlation coefficient of $R^2 > 0.99$ for the crystallization range between 0.25 and 0.75. This linearity means that the reaction mechanism is the same during the interval studied. In this case, a change in the activation energy is compensated by the same change in the logarithm of the pre-exponential factor. In this way, the reaction mechanism for any cooling rate can be determined.

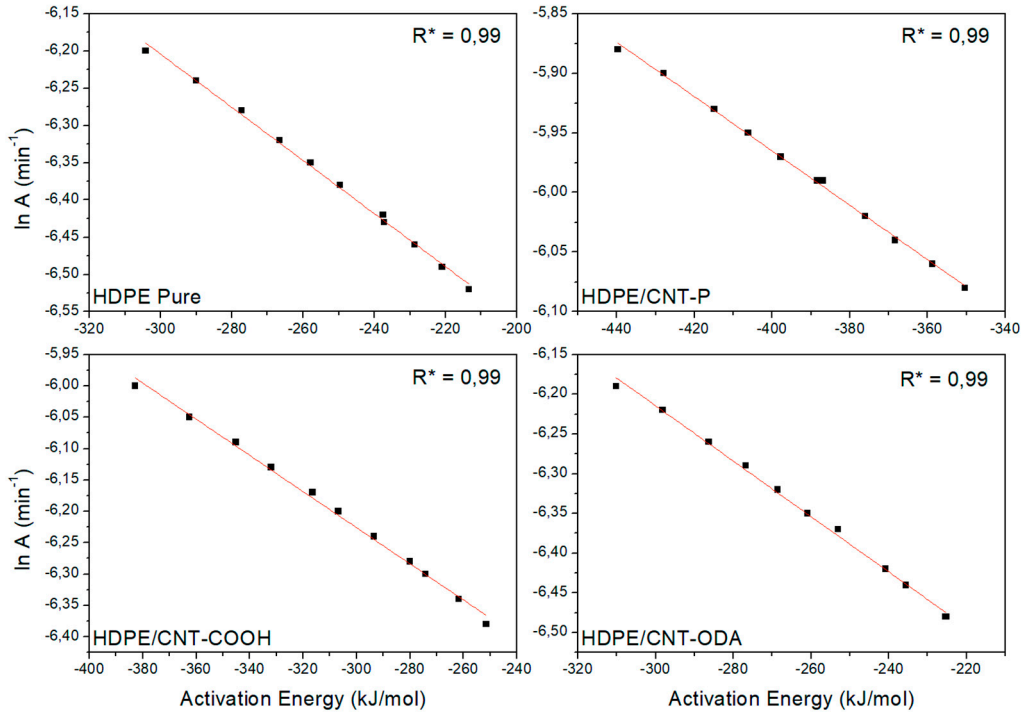

Figure 5. The compensation effect between E_a and ln$A$ for pure HDPE and HDPE/CNT nanocomposites.

The model and mechanism of crystallization of pure HDPE and HDPE/CNT nanocomposites was determined using the DSC curve with a cooling rate of 10 °C/min. Introducing E_a and A values into Equations (21) and (24), respectively, allowed the numerical determination of $y(\alpha)$ and $z(\alpha)$. Figure 6 shows the curves $y(\alpha)$ and $z(\alpha)$ for pure HDPE and HDPE/CNT nanocomposites.

The curves $y(\alpha)$ exhibit a maximum value (a_y) and the curves $z(\alpha)$ exhibit a minimum value (a_z), which are used for the determination of the crystallization mechanism. The values of a_y and a_z are compared with the values of the theoretical kinetics models in Figure 1. For all samples, a_z is approximately 0.633 and $0 < a_y < a_z$, showing that all the samples are crystallized by the Johnson-Mehl-Avrami (JMA) model of nucleation and growth. The JMA model is represented by Equation (26) [31]:

$$f(\alpha) = n(1-\alpha)\cdot[-\ln(1-\alpha)]^{1-1/n} \quad (26)$$

Substituting $f(\alpha)$ into Equation (21) results in Equation (27) below:

$$y(\alpha) = A\cdot n(1-\alpha)\cdot[-\ln(1-\alpha)]^{1-1/n} \quad (27)$$

The Avrami exponent "n" can be determined by fitting Equation (27) with experimental values of $y(\alpha)$ obtained from Figure 6. Figure 7 shows the curves $y(\alpha)$ fitted with Equation (27) for the pure HDPE and the HDPE/CNT nanocomposites. Note that the adjustment was performed

for the crystallization degree of 25% to 75% since the kinetic compensation was effective in this interval. The values of the Avrami coefficient "n" for pure HDPE and nanocomposites are shown in Table 3. A significant difference between the values of "n" for the neat HDPE when compared to the HDPE/CNT nanocomposites can be observed.

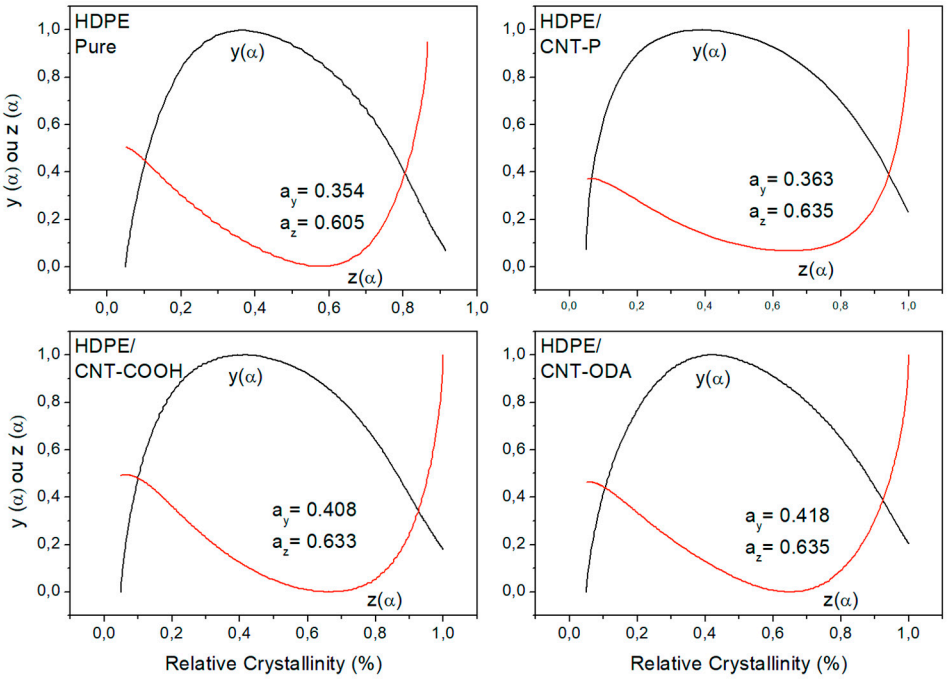

Figure 6. Experimental dependence of $y(\alpha)$ and $z(\alpha)$ versus α for pure HDPE and HDPE/CNT nanocomposites.

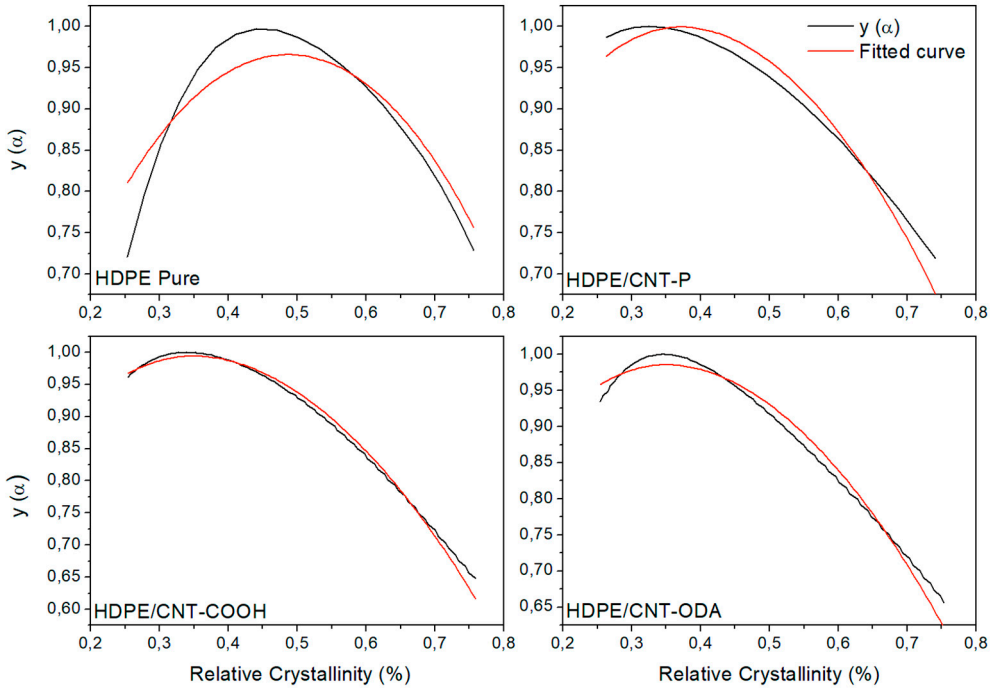

Figure 7. Curves of $y(\alpha)$ versus α normalized and fitted by Equation (27) for pure HDPE and HDPE/CNT nanocomposites.

Table 3. Avrami coefficient "n" of the empirical kinetic JMA model for pure HDPE and HDPE/CNT nanocomposites.

Sample	n
HDPE Pure	2.9
HDPE/CNT–P	1.9
HDPE/CNT–COOH	1.8
HDPE/CNT–ODA	1.8

The "n" value depends on the nucleation mechanism and geometry of crystal growth. For values between $1 \leq n \leq 2$, the growth will occur in one dimension (cylinders); for values between $2 \leq n \leq 3$, growth will occur in two dimensions (lamellae); and for values between $3 \leq n \leq 4$, growth will happen in three dimensions (spheres) [56], as summarized in Table 4.

Table 4. Values of "n" for different growth type and geometry of crystals [56].

n	Growth Type	Geometry
$5 \leq n \leq 6$	3 dimensions	Sheaf-like
$3 \leq n \leq 4$	3 dimensions	Spherulites
$2 \leq n \leq 3$	2 dimensions	Lamellas
$1 \leq n \leq 2$	1 dimension	Fibers

For pure HDPE (n = 2.9) the crystal growth occurs in two to three dimensions. The growth of a solid phase during polymer crystallization is initiated by the formation of nuclei, which develop in three dimensions, resulting in a spherulitic structure. Although the pure HDPE does not have reinforcing agents in its structure (seeds), the nucleation can occur by heterogeneities, such as impurities and partially melted molecules of the polymer [56]. The incorporation of carbon nanotubes into polyethylene decreased the values of "n" in about one unit (1.8 to 1.9). In this case, the nucleation process is not sporadic, as for the pure HDPE, but predetermined by the nanofillers (seeds).

At least two factors can affect the values of the Avrami coefficient. One factor is related to the crystallization rate of the polymer. Higher cooling rates prevent the complete formation of spherulites, reducing the value of "n". Another factor is the growth site impingement that can modify the crystal growth mechanism. The addition of seeds into a polymer will increase the number of nucleation sites and, consequently, the crystalline volume fractions. Thus, the effect of impingement and truncation of crystal sites decreases the crystallization rate, reducing "n" [56].

Some studies have already reported that the addition of organic and inorganic particles can accelerate the isothermal and non-isothermal crystallization of HDPE, reducing the Avrami coefficient [55,57,58]. In this way, the carbon nanotubes will act as nucleating agents, creating various nuclei that will grow and, consequently, imitates the grow of one another. The mutual interference of these crystallization localities occurs before the spherulitic structure can develop, resulting in a very fine-grained structure [59].

There are also indications that lower "n" values occur when the final size of the growth units is small, which means the growth units formed during the "seed" crystallization are smaller than those produced in seedless crystallizations. In other words, lower values of "n" may occur when the polymer structure is granular, being formed by many small growth units [60].

Despite the reduction in the value of "n" and the difference in size and shape of crystal growth with the incorporation of CNTs, the crystallization of pure HDPE and HDPE/CNT nanocomposites are similar in some respects. For all samples, the crystallization mechanism was the same (JMA) and the absolute crystallinity degree was similar.

4.2. Polarized Optical Microscopy (POM)

The characterization using POM was carried out to verify the results obtained by the kinetic calculations. Figure 8 shows the POM images of pure HDPE at 127 °C isotherm at various times. Figure 8a shows the melted polyethylene before starting the crystallization process. Figure 8b shows the first nucleation sites occurred with two types of nuclei growth. One in the form of lamellae (two dimensions) and the other in the form of spherulites (three dimensions). Then, from Figure 8c the transformation of lamellas into the spherulitic structure and the growth of the previously formed spherulites can be observed. In the next steps (Figure 8d,e), the spherulites continue to grow until complete crystallization, producing the final structure (Figure 8f).

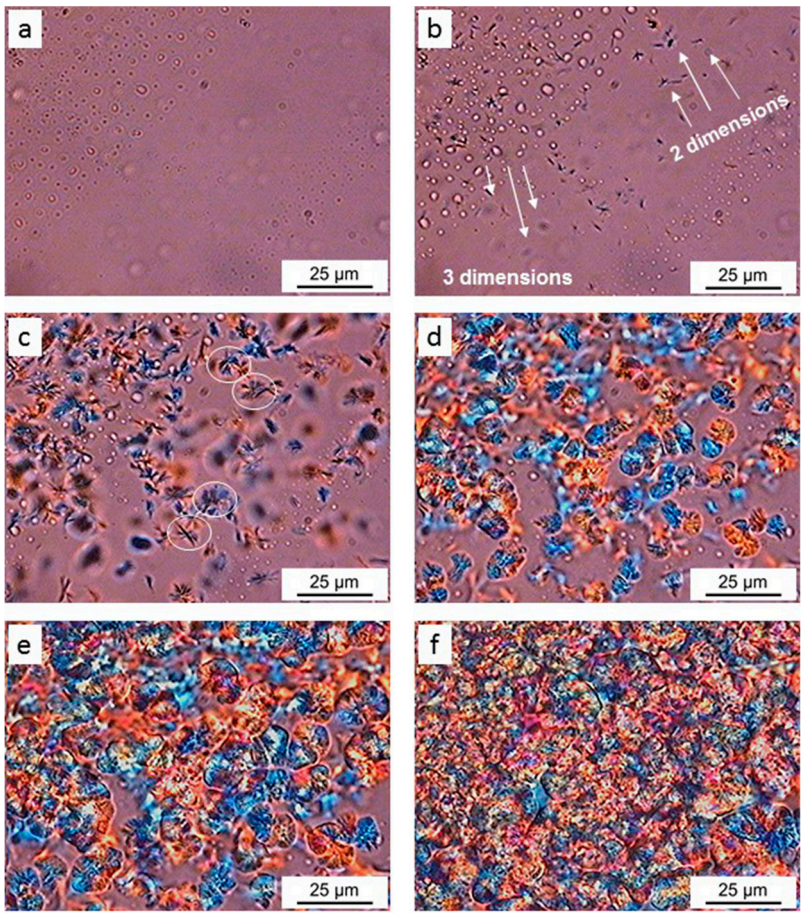

Figure 8. Polarized optical microscopy (POM) images of pure HDPE at 127 °C isotherm: (**a**) 30 s, (**b**) 2 min, (**c**) 5 min, (**d**) 8 min, (**e**) 10 min, and (**f**) 15 min.

For pure HDPE, both two- and three-dimensional nuclei are formed at the beginning of crystallization, showing that distinct mechanisms are simultaneously occurring. Due to this factor, the curve fitting for polyethylene shown in Figure 7 is less accurate when compared to nanocomposites. The two-dimensional nuclei grow to spherulitic structure with the crystallization process. The spherulites increase until reaching total crystallization. The final structure consists of large spherulites (15–20 µm in diameter), in agreement with Avrami's coefficient (n = 2.9).

Figure 9 shows POM images of HDPE/CNT nanocomposites at 127 °C isotherm after 5 and 15 min. For all nanocomposite samples the nucleation sites begin to appear at about 5 min and the final structure is rapidly formed (15 min). The presence of CNTs, functionalized or not, significantly increased the number of nucleation sites, reducing the size of crystallites. The identification of each nucleus growth separately is not possible, since various crystallization sites appeared simultaneously. However,

the perpendicular crystallite growths to nanotube cluster (dark parts) can be observed. In general, the incorporation of CNTs induces the growth of the polymer chains in directions perpendicular to the length of the CNTs. This result is in agreement with Avrami's coefficient, which showed that the crystallite growth occurs in the form of lamellas, in two dimensions [18].

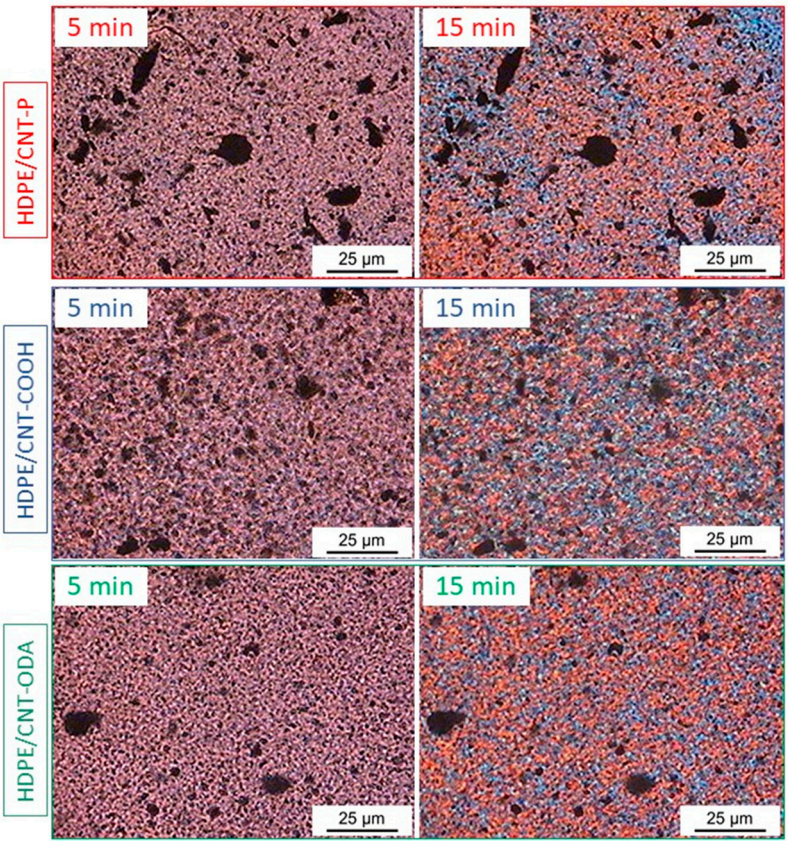

Figure 9. POM images of HDPE/CNT nanocomposites at 127 °C isotherm.

5. Conclusions

The effect of functionalized and non-functionalized CNTs on HDPE crystallization kinetic was studied by the isoconversional method. The results showed that the addition of CNT–P and CNT–COOH drastically reduced *Ea*, while CNT–ODA caused a slight reduction. The similarity of ODA and HDPE chains, besides the polarity, increased the dispersion and interaction of this filler with the matrix. In this way, CNT–ODA merged with the matrix, reducing its activity as a nucleating agent. Although all CNTs reduced *Ea* and changed the values of *Tp* and *Ton* when compared to pure HDPE, the crystallization mechanism and the absolute crystallinity was the same for all the samples. Both pure HDPE and HDPE/CNTs nanocomposites crystallized by the model proposed by Johnson-Mehl-Avrami (JMA). In relation to the absolute crystallinity degree, CNTs induced the formation of more nucleation sites but hindered the mobility of the polymeric chains. Thus, CNTs had no significant effect on nanocomposites absolute crystallinity, remaining the same when compared with pure HDPE. The values obtained for the Avrami coefficients with the POM images showed that the pure HDPE started its crystallization with crystals of two and three dimensions. The final structure was composed of large spherulites. On the other hand, for the nanocomposites, the crystallization occurred quickly, with the emergence of several simultaneous nucleation sites that resulted in a structure constituted of finer crystals. The results obtained proved the effectiveness of the isoconversional method for the kinetic crystallization study of HDPE and HDPE/CNTs nanocomposites.

Author Contributions: Conceptualization, B.R.C.d.M., T.M.B.C. and G.P.T.; Data curation, B.R.C.d.M., T.M.B.C. and R.G.R.; Formal analysis, B.R.C.d.M., T.L.d.A.M. and R.G.R.; Funding acquisition, G.P.T.; Investigation, B.R.C.d.M.; Methodology, B.R.C.d.M., T.M.B.C. and G.P.T.; Project administration, B.R.C.d.M. and G.P.T.; Resources, G.P.T.; Software, B.R.C.d.M. and T.M.B.C.; Supervision, L.d.S.C. and G.P.T.; Validation, L.d.S.C. and G.P.T.; Visualization, G.P.T.; Writing—original draft, B.R.C.d.M.; Writing—review and editing, T.M.B.C., T.L.d.A.M., L.d.S.C. and G.P.T.

Funding: This research was funded by the Brazilian institutions CAPES (Coordenação de Aperfeiçoamento de Pessoal de Nível Superior) and FAPESP (Fundação de Amparo à Pesquisa do Estado de São Paulo, Grant: 2014/17492-6).

Conflicts of Interest: The authors declare no conflict of interest.

References

1. Geyer, R.; Jambeck, J.R.; Law, K.L. Production, use, and fate of all plastics ever made. *Sci. Adv.* **2017**, *3*, 1–5. [CrossRef]
2. Dordinejad, A.K.; Sharif, F.; Ebrahimi, M.; Rashedi, R. Rheological and Thermorheological Assessment of Polyethylene in Multiple Extrusion Process. *Thermochim. Acta* **2018**, *668*, 19–27. [CrossRef]
3. Peacock, A. *Handbook of Polyethylene: Structures: Properties, and Applications*; CRC Press: New York, NY, USA, 2000.
4. Roumeli, E.; Pavlidou, E.; Bikiaris, D.; Chrissafis, K. Microscopic observation and micromechanical modeling to predict the enhanced mechanical properties of multi-walled carbon nanotubes reinforced crosslinked high density polyethylene. *Carbon* **2014**, *67*, 475–487. [CrossRef]
5. Mahfuz, H.; Adnan, A.; Rangari, V.K.; Jeelani, S. Manufacturing and characterization of carbon nanotube/polyethylene composites. *Int. J. Nanosci.* **2005**, *4*, 55–72. [CrossRef]
6. Monthioux, M.; Kuznetsov, V.L. Who should be given the credit for the discovery of carbon nanotubes? *Carbon* **2006**, *44*, 1621–1623. [CrossRef]
7. Iijima, S. Helical microtubules of graphitic carbon. *Nature* **1991**, *354*, 56. [CrossRef]
8. De Volder, M.F.; Tawfick, S.H.; Baughman, R.H.; Hart, A.J. Carbon nanotubes: Present and future commercial applications. *Science* **2013**, *339*, 535–539. [CrossRef] [PubMed]
9. Pop, E.; Mann, D.; Wang, Q.; Goodson, K.; Dai, H. Thermal conductance of an individual single-wall carbon nanotube above room temperature. *Nano Lett.* **2006**, *6*, 96–100. [CrossRef] [PubMed]
10. He, H.; Pham-Huy, L.A.; Dramou, P.; Xiao, D.; Zuo, P.; Pham-Huy, C. Carbon nanotubes: Applications in pharmacy and medicine. *BioMed Res. Int.* **2013**, *2013*, 578290. [CrossRef] [PubMed]
11. Xie, X.-L.; Mai, Y.-W.; Zhou, X.-P. Dispersion and alignment of carbon nanotubes in polymer matrix: A review. *Mater. Sci. Eng. R* **2005**, *49*, 89–112. [CrossRef]
12. Liu, X.-C.; Choi, J.-W. Improved dispersion of carbon nanotubes in polymers at high concentrations. *Nanomaterials (Basel)* **2002**, *2*, 329–347. [CrossRef]
13. Kim, J.; Hong, S.M.; Kwak, S.; Seo, Y. Physical properties of nanocomposites prepared by in situ polymerization of high-density polyethylene on multiwalled carbon nanotubes. *Phys. Chem. Chem. Phys.* **2009**, *11*, 10851–10859. [CrossRef]
14. Bekyarova, E.; Ni, Y.; Malarkey, E.B.; Montana, V.; McWilliams, J.L.; Haddon, R.C.; Parpura, V. Applications of carbon nanotubes in biotechnology and biomedicine. *J. Biomed. Nanotechnol.* **2005**, *1*, 3–17. [CrossRef]
15. De Menezes, B.R.C.; Rodrigues, K.F.; Fonseca, B.C.S.; Ribas, R.G.; Montanheiro, T.L.A.; Thim, G.P. Recent advances in the use of carbon nanotubes as smart biomaterials. *J. Mater. Chem. B* **2019**. [CrossRef]
16. Carrión, F.J.; Espejo, C.; Sanes, J.; Bermúdez, M.D. Single-walled carbon nanotubes modified by ionic liquids as antiwear additives of thermoplastics. *Compos. Sci. Technol.* **2010**, *70*, 2160–2167. [CrossRef]
17. De Menezes, B.R.C.; Ferreira, F.V.; Silva, B.C.; Simonetti, E.A.N.; Bastos, T.M.; Cividanes, L.S.; Thim, G.P. Effects of octadecylamine functionalization of carbon nanotubes on dispersion, polarity, and mechanical properties of CNT/HDPE nanocomposites. *J. Mater. Sci.* **2018**, *53*, 14311–14327. [CrossRef]
18. Grady, B.P. Effects of carbon nanotubes on polymer physics. *J. Polym. Sci. B Polym. Phys.* **2012**, *50*, 591–623. [CrossRef]
19. Vaughan, A.S.; Hosier, I.L. The effect of dibenzylidene sorbitol on the crystallization behaviour of polyethylene. *J. Mater. Sci.* **2008**, *43*, 2922–2928. [CrossRef]

20. Zhang, C.; Yi, X.-S.; Asai, S.; Sumita, M. Morphology, crystallization and melting behaviors of isotactic polypropylene/high density polyethylene blend: Effect of the addition of short carbon fiber. *J. Mater. Sci.* **2000**, *35*, 673–683. [CrossRef]
21. Tarani, E.; Wurm, A.; Schick, C.; Bikiaris, D.N.; Chrissafis, K.; Vourlias, G. Effect of graphene nanoplatelets diameter on non-isothermal crystallization kinetics and melting behavior of high density polyethylene nanocomposites. *Thermochim. Acta* **2016**, *643*, 94–103. [CrossRef]
22. Shehzad, F.; Thomas, S.P.; Al-Harthi, M.A. Non-isothermal crystallization kinetics of high density polyethylene/graphene nanocomposites prepared by in-situ polymerization. *Thermochim. Acta* **2014**, *589*, 226–234. [CrossRef]
23. Sahoo, R.K.; Panda, B.P.; Nayak, S.K.; Mohanty, S. Mechanical and morphological investigation of virgin polyethylene and silver nanoparticle-loaded nanocomposites film: Comprehensive analysis of kinetic models for non-isothermal crystallization. *Bull. Mater. Sci.* **2017**, *40*, 307–320. [CrossRef]
24. Fan, Y.; Lou, J.; Jamali, J.; Lu, Y.; Wood, J. Effect of Clay Dispersion on the Nonisothermal and Isothermal Crystallization Behaviors of Polyethylene Composites. *Polym. Plast. Technol. Eng.* **2017**, *56*, 1646–1656. [CrossRef]
25. Khawam, A.; Flanagan, D.R. Complementary Use of Model-Free and Modelistic Methods in the Analysis of Solid-State Kinetics. *J. Phys. Chem. B* **2005**, *109*, 10073–10080. [CrossRef] [PubMed]
26. Khawam, A.; Flanagan, D.R. Role of isoconversional methods in varying activation energies of solid-state kinetics: II. Nonisothermal kinetic studies. *Thermochim. Acta* **2005**, *436*, 101–112. [CrossRef]
27. Vyazovkin, S. Advanced isoconversional method. *J. Therm. Anal.* **1997**, *49*, 1493–1499. [CrossRef]
28. Cividanes, L.S.; Brunelli, D.D.; Bertran, C.A.; Campos, T.M.B.; Thim, G.P. Urea effect on the mechanism of mullite crystallization. *J. Mater. Sci.* **2011**, *46*, 7384–7392. [CrossRef]
29. Sharp, J.H.; Brindley, G.W.; Achar, B.N.N. Numerical Data for Some Commonly Used Solid State Reaction Equations. *J. Am. Ceram. Soc.* **1996**, *49*, 379–382. [CrossRef]
30. Criado, J.M.; Málek, J.; Gotor, F.J. The applicability of the Šesták-Berggren kinetic equation in constant rate thermal analysis (CRTA). *Thermochim. Acta* **1990**, *158*, 205–213. [CrossRef]
31. Málek, J.; Mitsuhashi, T. Testing Method for the Johnson–Mehl–Avrami Equation in Kinetic Analysis of Crystallization Processes. *J. Am. Ceram. Soc.* **2004**, *83*, 2103–2105. [CrossRef]
32. Koga, N.; Malek, J. Accommodation of the actual solid-state process in the kinetic model function. *Part 2. Applicability of the empirical kinetic model function to diffusion-controlled reactions, Thermochim. Acta* **1996**, *282–283*, 69–80. [CrossRef]
33. Málek, J.; Sesták, J.; Rouquerol, F.; Rouquerol, J.; Criado, J.M.; Ortega, A. Possibilities of two non-isothermal procedures (temperature- or rate-controlled) for kinetical studies. *J. Therm. Anal.* **1992**, *38*, 71–87. [CrossRef]
34. Janković, B.; Adnađević, B.; Jovanović, J. Application of model-fitting and model-free kinetics to the study of non-isothermal dehydration of equilibrium swollen poly (acrylic acid) hydrogel: Thermogravimetric analysis. *Thermochim. Acta* **2007**, *452*, 106–115. [CrossRef]
35. Vyazovkin, S.; Wight, C.A. Kinetics in solids. *Annu. Rev. Phys. Chem.* **1997**, *48*, 125–149. [CrossRef] [PubMed]
36. Azimi, H.R.; Rezaei, M.; Abbasi, F.; Charchi, A.; Bahluli, Y. Non-isothermal degradation kinetics of MMA-St copolymer and EPS lost foams. *Thermochim. Acta* **2008**, *474*, 72–77. [CrossRef]
37. Laidler, K.J. The development of the Arrhenius equation. *J. Chem. Educ.* **1984**, *61*, 494. [CrossRef]
38. Doyle, C.D. Estimating isothermal life from thermogravimetric data. *J. Appl. Polym. Sci.* **1962**, *6*, 639–642. [CrossRef]
39. Zeman, S. Kinetic compensation effect and thermolysis mechanisms of organic polynitroso and polynitro compounds. *Thermochim. Acta* **1997**, *290*, 199–217. [CrossRef]
40. Erceg, M.; Kovačić, T.; Perinović, S. Kinetic analysis of the non-isothermal degradation of poly(3-hydroxybutyrate) nanocomposites. *Thermochim. Acta* **2008**, *476*, 44–50. [CrossRef]
41. López-Fonseca, R.; Landa, I.; Gutiérrez-Ortiz, M.A.; González-Velasco, J.R. Non-isothermal analysis of the kinetics of the combustion of carbonaceous materials. *J. Therm. Anal. Calorim.* **2005**, *80*, 65–69. [CrossRef]
42. Ozawa, T. A New Method of Analyzing Thermogravimetric Data. *Bull. Chem. Soc. Jpn.* **1965**, *38*, 1881–1886. [CrossRef]
43. Ozawa, T. Non-isothermal kinetics and generalized time. *Thermochim. Acta* **1986**, *100*, 109–118. [CrossRef]

44. Gotor, F.J.; Criado, J.M.; Malek, J.; Koga, N. Kinetic Analysis of Solid-State Reactions: The Universality of Master Plots for Analyzing Isothermal and Nonisothermal Experiments. *J. Phys. Chem. A* **2000**, *104*, 10777–10782. [CrossRef]
45. Koga, N. Kinetic analysis of thermoanalytical data by extrapolating to infinite temperature. *Thermochim. Acta* **1995**, *258*, 145–159. [CrossRef]
46. Antunes, E.F.; Almeida, E.C.; Rosa, C.B.; de Medeiros, L.I.; Pardini, L.C.; Massi, M.; Corat, E.J. Thermal annealing and electrochemical purification of multi-walled carbon nanotubes produced by camphor/ferrocene mixtures. *J. Nanosci. Nanotechnol.* **2010**, *10*, 1296–1303. [CrossRef] [PubMed]
47. Manchado, M.A.L.; Valentini, L.; Biagiotti, J.; Kenny, J.M. Thermal and mechanical properties of single-walled carbon nanotubes–polypropylene composites prepared by melt processing. *Carbon* **2005**, *43*, 1499–1505. [CrossRef]
48. Ferreira, F.V.; Franceschi, W.; Menezes, B.R.C.; Brito, F.S.; Lozano, K.; Coutinho, A.R.; Cividanes, L.S.; Thim, G.P. Dodecylamine functionalization of carbon nanotubes to improve dispersion, thermal and mechanical properties of polyethylene based nanocomposites. *Appl. Surf. Sci.* **2017**, *410*, 267–277. [CrossRef]
49. Cheng, J.; Pu, H.; Du, J. A processing method with high efficiency for low density polyethylene nanofibers reinforced by aligned carbon nanotubes via nanolayer coextrusion. *Polymer* **2017**, *111*, 222–228. [CrossRef]
50. Kim, J.; Kwak, S.; Hong, S.M.; Lee, J.R.; Takahara, A.; Seo, Y. Nonisothermal Crystallization Behaviors of Nanocomposites Prepared by In Situ Polymerization of High-Density Polyethylene on Multiwalled Carbon Nanotubes. *Macromolecules* **2010**, *43*, 10545–10553. [CrossRef]
51. Bakshi, S.R.; Tercero, J.E.; Agarwal, A. Synthesis and characterization of multiwalled carbon nanotube reinforced ultra high molecular weight polyethylene composite by electrostatic spraying technique. *Compos. Part A Appl. Sci. Manuf.* **2007**, *38*, 2493–2499. [CrossRef]
52. Ferreira, C.I.; Dal Castel, C.; Oviedo, M.A.S.; Mauler, R.S. Isothermal and non-isothermal crystallization kinetics of polypropylene/exfoliated graphite nanocomposites. *Thermochim. Acta* **2013**, *553*, 40–48. [CrossRef]
53. Seo, Y.; Kim, J.; Kim, K.U.; Kim, Y.C. Study of the crystallization behaviors of polypropylene and maleic anhydride grafted polypropylene. *Polymer* **2000**, *41*, 2639–2646. [CrossRef]
54. Venkatesh, M.; Ravi, P.; Tewari, S.P. Isoconversional Kinetic Analysis of Decomposition of Nitroimidazoles: Friedman method vs Flynn–Wall–Ozawa Method. *J. Phys. Chem. A* **2013**, *117*, 10162–10169. [CrossRef] [PubMed]
55. Ou, R.; Guo, C.; Xie, Y.; Wang, Q. Non-isothermal crystallization kinetics of kevlar fiber-reinforced wood flour/HDPE composites. *BioResources* **2011**, *6*, 4547–4565.
56. Mandelkern, L. *Crystallization of Polymers: Kinetics and Mechanisms*, 2nd ed.; Cambridge University Press: Cambridge, UK, 2004; pp. 11–27.
57. Odian, G. *Principles of Polymerization*, 4th ed.; John Wiley & Sons: New York, NY, USA, 2004; pp. 301–302, 696–697.
58. Zou, P.; Tang, S.; Fu, Z.; Xiong, H. Isothermal and non-isothermal crystallization kinetics of modified rape straw flour/high-density polyethylene composites. *Int. J. Therm. Sci.* **2009**, *48*, 837–846. [CrossRef]
59. Hartley, F.; Lord, F.; Morgan, L. Crystallization phenomena in polymers—Effect of melt conditions and the temperature of crystallization on the course of the crystallization in polyethylene terephthalate. *Philos. Trans. R. Soc. A* **1954**, *247*, 23–34. [CrossRef]
60. Banks, W.; Gordon, M.; Sharples, A. The crystallization of polyethylene after partial melting. *Polymer* **1963**, *4*, 289–302. [CrossRef]